RSC Advances

ROYAL SOCIETY OF CHEMISTRY

www.rsc.org/advances

Journal Name

COMMUNICATION

Diverse Redox Chemistry of Photo/Ferrioxalate System

Zhaohui Wang*, Dongxue Xiao and Jianshe Liu

The diverse redox processes of photo/ferrioxalate system (PFS) were investigated by varying the concentrations of Fe(III), oxalate and oxygen. Photoreactivity of PFS is determined by the prevalence of the most photolabile Fe(III) and abundance of Fe(III) and oxalate, which is critical for operation optimization of PFS in wastewater treatment.

Introduction

Ferrioxalate complex, first known as a chemical actinometer, recently finds its photochemical application in wastewater treatment.[1-4] Various reactive intermediates, such as Fe(II) and reactive oxygen species (ROS) including $O_2^{\bullet-}$, $^{\bullet}OH$ and H_2O_2, are generated with Fe(III)-oxalate complexes (photo/ferrioxalate system, PFS) being photolyzed (Eqs. 1-7).[5-9] Photoproduced $^{\bullet}OH$ is significant for the oxidative decontamination of organic substances in natural and engineered systems.[1,6,9] The high treatment efficiency can be sustained with UV irradiation in the presence of excess oxalate.

$$[Fe(Ox)_3]^{3-} \xrightarrow{hv} [Fe(Ox)_2]^- + 2CO_2^{\bullet-} \quad (1)$$

$$[Fe(Ox)_3]^{3-} \xrightarrow{hv} [Fe(Ox)_2]^{2-} + C_2O_4^{\bullet-} \quad (2)$$

$$CO_2^{\bullet-} + [Fe(Ox)_3]^{3-} \longrightarrow [Fe(Ox)_2]^{2-} + CO_2 + C_2O_4^{2-} \quad (3)$$

$$CO_2^{\bullet-} + O_2 \longrightarrow CO_2 + O_2^{\bullet-} \quad (4)$$

$$O_2^{\bullet-} + H^+ \longleftrightarrow HO_2^{\bullet} \quad (5)$$

$$2HO_2^{\bullet} \longrightarrow H_2O_2 + O_2 \quad (6)$$

$$Fe(II) + H_2O_2 \longrightarrow Fe(III) + {}^{\bullet}OH + OH^- \quad (7)$$
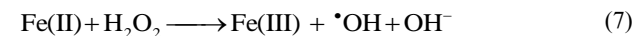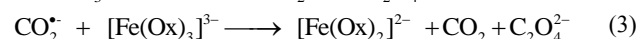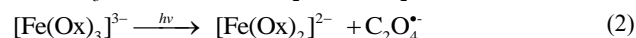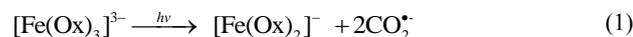
Although the application of PFS in water purification is well-known, the mechanism of photolysis and subsequent reactions in PFS remains controversial.[7-9] There are two different basic ideas on the mechanism of the primary photolysis reaction of ferrioxalate. Excitation of ferrioxalate is followed by photodissolution without electron transfer between iron and oxalate ligand (Eq.1)[7], or by an intramolecular ligand-to-metal charge transfer (LMCT) process (Eq.2).[5,6,8] Despite a debatable argument on the two pathways, both mechanisms will lead to the formation of Fe(II) and at least one radical anion ($C_2O_4^{\bullet-}/CO_2^{\bullet-}$). $CO_2^{\bullet-}$ is a strong reducing agent (E^0=-1.8 V vs NHE) and can react with another ferrioxalate molecule or instead reduce O_2 to superoxide anion ($O_2^{\bullet-}$) at near-diffusion-controlled rate ($k = 2.4 \times 10^9 \, M^{-1} \, s^{-1}$).[10] Oxalate can form three kinds of complex with Fe(III), $Fe(Ox)^+$, $Fe(Ox)_2^-$ and $Fe(Ox)_3^{3-}$, with different proportions depending on the pH and the Fe(III)-to-oxalate ratio. Vincze and Papp[11] measured quantum yields at 254 nm of 0, 1.18 and 1.60 for $Fe(Ox)^+$, $Fe(Ox)_2^-$ and $Fe(Ox)_3^{3-}$, respectively. In view of their markedly different photoactivity, a diverse photoredox chemistry of PFS is expected with the changes in Fe speciation caused by rapid consumption of oxalate. However, most of related work was done in the presence of excess oxalate.[1-7] Few investigations focus on the photochemistry of PFS at low Fe(III)/oxalate ratio to resemble the scenario of oxalate depletion, despite its importance in understanding the fundamental reaction mechanism and practical operation.

In this study, the photoredox processes of PFS at different Fe(III)/oxalate ratios was investigated by determining the photoproduction of Fe(II) and H_2O_2. AO7, a non-biodegradable organic pollutant, was selected to probe the $^{\bullet}OH$ photoproduction. A preliminary mechanism was proposed based on the results of Fe speciation and Electron spin resonance (ESR).

Experimental section

Chemicals

Iron(III) perchlorate hydrate and Acid Orange 7 (AO7: $C_{16}H_{11}N_2O_4SNa$) were purchased from Aldrich. 5, 5-dimethyl-1-pyrroline-*N*-oxide (DMPO) and N, N-Diethyl-p-phenylenediamine (DPD) were from Sigma Chemical Co. Horseradish peroxidase (POD) was purchased from Huamei Biologic Engineering, China. Oxalic acid (Ox), sodium hydroxide, perchloric acid, potassium phosphate monobasic (KH_2PO_4), sodium phosphate monobasic (NaH_2PO_4) and 1, 10-phenanthroline, were of reagent grade and used as supplied. Barnstead UltraPure water (18.3 MΩ cm) was used for all experiments.

Experimental procedures

All photochemical experiments were conducted in a 70 mL cylindrical Pyrex vessel (3.8 cm diameter, containing 50 mL solution) under continuous magnetic stirring. The ultraviolet irradiation source was a 100 W Hg lamp (Toshiba SHL-100UVQ-2) as specified elsewhere.[12] The UV light, which had wavelengths below 290 nm, was filtered with the Pyrex glass. The reaction mixture for photolysis was freshly prepared by dilution of stock solutions of 0.01 M oxalic acid, 5 mM Fe(III) at pH 1.5 ($HClO_4$). AO7 (50 μM) was used as a probe compound for hydroxyl radicals. The initial pH was adjusted with dilute $HClO_4$ or NaOH. The pH

variations during all experiments were less than ±0.2 pH units. Deaeration, when desired, was accomplished by argon bubbling for at least 20 min before irradiation and throughout the experiments. During the each kinetic experiment, 1 mL (for determination of Fe(II) and H_2O_2) or 2 mL (for dye measurement) aliquots were sampled with a new syringe each time and immediately disposed for the consequent analysis.

Methods and Analysis

The concentration of Fe(II) was monitored spectrophotometrically by a modified phenanthroline method.[12,13] H_2O_2 determination was performed using a POD/DPD method.[14] The dye decoloration was monitored by measuring the absorbance at 485 nm on a Hitachi U-2900 spectrophotometer.[15] The photodegradation rates were well described by pseudo-first-order model. TOC was determined on a Tekmar Dohrmann Apllo 9000 TOC analyzer. ESR spectra of DMPO spin-trapping radicals were recorded at room temperature on a Bruker EPR ELEXSYS 500 spectrometer equipped with an *in situ* irradiation source (a Quanta-Ray ND:YAG laser system λ=355 nm). The simulations of ESR spectra were obtained with the use of WinSim EPR simulation software. The spin adduct assignment was based on its distinctive hyperfine splitting parameters (similarity>90%). The detailed parameters were reported previously.[12] Fe speciation was calculated using the MEDUSA software, a chemical equilibrium program with a built-in thermodynamic database.[16]

Results and discussion

Formation of H_2O_2 and Fe(II)

H_2O_2 and Fe(II) are the major long-lived photolyzed products of Fe(III)-oxalato complexes.[5] Their concentrations at different concentrations of Fe(III) and oxalate (Fe(III), 100 and 200 μM; oxalate, 100-1000 μM) were monitored (Fig.1). Fig.1a shows that amount of H_2O_2 only can be measured at the low Fe(III) concentration during 30 min of irradiation. It should be noted that all the concentrations of H_2O_2 measured were accumulated concentrations, that is, these just represented the net outcome of H_2O_2 formed and decomposed by a subsequent rapid dark reaction with residual Fe(II).[5] Therefore, no evidence of H_2O_2 accumulation at 200 μM Fe(III) did not mean no formation of H_2O_2, but probably indicated a rapid consumption of H_2O_2 after formation.

Fig.1b shows that a large amount of Fe(II) was generated at 200 μM Fe(III), with the consumption of oxalate (Fig. S1), indicating that a typical photolysis proceeded even at a high Fe(III) level. Since Fe(II)-oxalate complex (k= 3.1×10^4 $M^{-1}s^{-1}$) reacts with H_2O_2 three orders of magnitude faster than Fenton reaction (k=53-76 M^{-1} s^{-1})[17], the newly generated H_2O_2 was expected to be rapidly consumed by Fe(II). Therefore, the extremely low levels of H_2O_2 at high Fe(III) dosage should not be ascribed to the poor photoreactivity of Fe(III)-oxalate complex, but should be partially resulted from the rapid decomposition of H_2O_2.

AO7 degradation kinetics

The most important feature of PFS is efficient generation of highly reactive $^\bullet$OH radicals.[1-3] The photoproduction of $^\bullet$OH was determined with the addition of AO7 as a $^\bullet$OH scavenger ($k_{^\bullet OH+AO7}$=(1.10±0.04)×10^{10} M^{-1} s^{-1}).[18] The reaction of AO7 with $CO_2^{\bullet-}$ is not considered under aerated conditions because of the rapid quenching reaction of $CO_2^{\bullet-}$ by molecular oxygen.[10] Fig.2 demonstrates the variation of degradation rates (k, min^{-1}) at the different Fe(III)/oxalate concentrations. Interestingly, each k profile shows a "V" shape curve, with a reflection point (minimum degradation rate) at 50 μM oxalate for 100 μM Fe(III), 100 μM oxalate for 200 μM Fe(III) and 20 μM oxalate for 400 μM Fe(III), respectively. There were no obvious changes of k at Fe(III) concentration below 200 μM. The degradation rate of AO7 decreased at 400 μM Fe(III) and high oxalate loading (>200 μM). This clearly

indicates that addition of excess reactants (i.e. Fe(III), oxalate) would not always lead to an enhanced degradation rate. To maintain the high efficiency of PFS, it is recommended to always keep oxalate concentration above the reflection points in the solution for the specific Fe(III) loading.
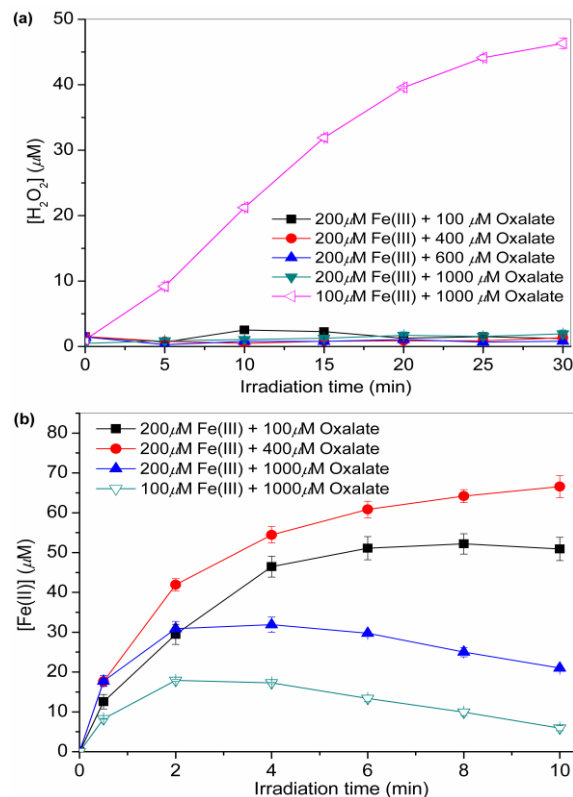
Fig. 1. (a) H_2O_2 and (b) Fe(II) photoproduction as a function of irradiation time. pH 3.0.
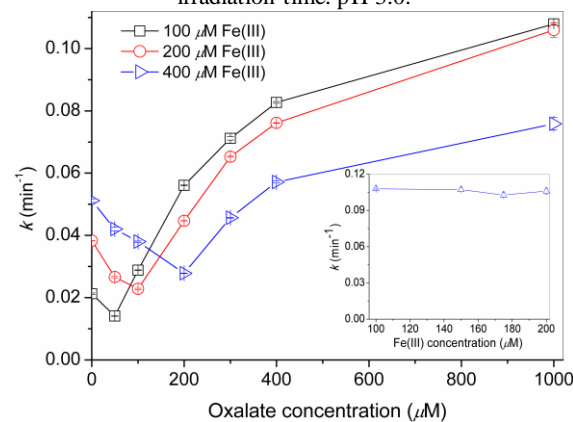
Fig. 2. The degradation rate of AO7 as function of oxalate concentration at pH 3.0. *Inset*: variation of k with initial Fe(III) concentration. AO7, 50 μM.

Fe(III) speciation

Photoproduction of $^\bullet$OH, as reflected by photodegradation efficiency of AO7, should be closely associated with the photoreactivity of Fe complexes and Fe speciation. Fig. 3 shows the speciation of Fe(III) as a function of total oxalate concentration ($[Ox^{2-}]_T$) at pH 3.0. With the increasing concentration of oxalate over the range of 0-1000 μM, the Fe speciation gradually changes with an increasing amount of Fe(III)-oxalato complexes accompanied by a decreasing amount of hexaaquo and hydroxylated Fe(III) complexes (i.e. Fe^{3+}, $FeOH^{2+}$, $FeOH_2^+$). Mon(oxalato)

complex (Fe(Ox)$^+$) is the predominant species of Fe(III)-oxalato complexes at 1:1 of Fe(III)-to-oxalate ratio, whereas Fe(Ox)$_2^-$ and Fe(Ox)$_3^{3-}$ are the major species at Fe(III):oxalate<1:2. Since Fe(Ox)$_2^-$ and Fe(Ox)$_3^{3-}$ are much more efficiently photolyzed than Fe(Ox)$^+$ and FeOH^{2+},[11] the Fe(II) quantum yield, a collective value contributed by each photolabile Fe complexes, should vary significantly at different Fe(III)/oxalate concentrations.
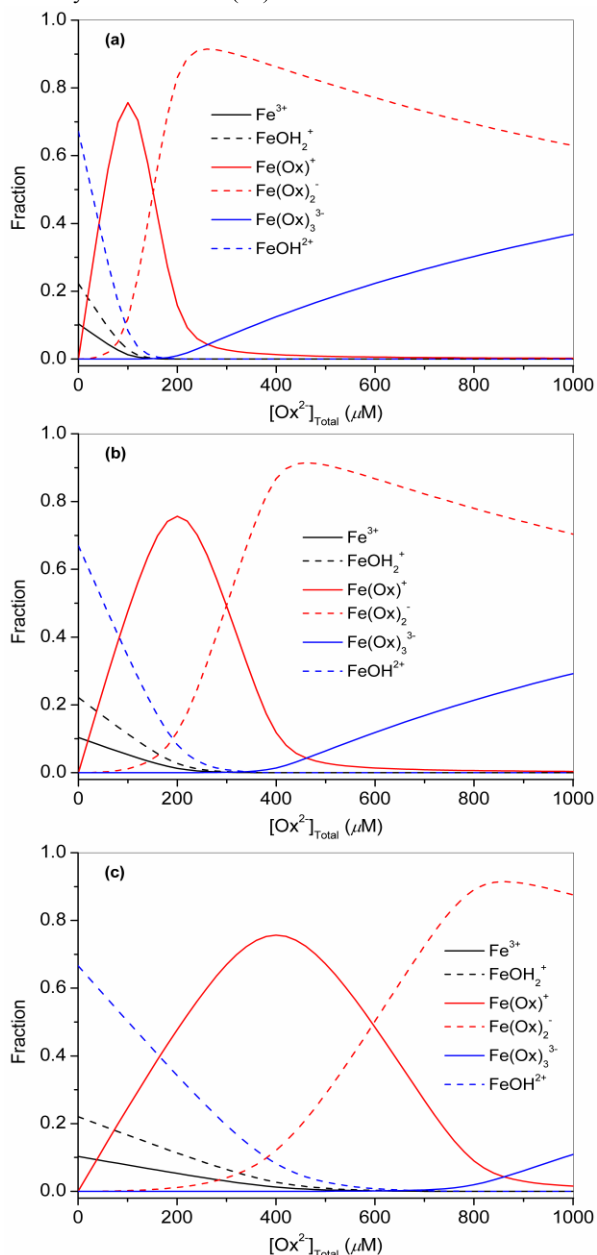
Fig. 3. Molar fraction distribution of the Fe(III)-Ox complexes at different Fe(III) concentrations: (a) 100 μM; (b) 200 μM; (c) 400 μM. pH 3.0.

Due to the difficulty to obtain the quantum yield of each photolabile species within the range of 300-400 nm,[19] here quantum yields at the main emission wavelength (366 nm) of Hg lamp were used to approximately evaluate the reactivity under polychromatic irradiation as used in the study. Because of their similar nLpOH-dLMCT absorption, FeOH$_2^+$ was assumed to have roughly close photoreduction reactivity to that of FeOH^{2+} ($\Phi_{366\,nm} \approx 0.017$)[20,21], and therefore was regarded equivalent to FeOH^{2+} in this study. According

to recently reported values by Weller et al.[19], Fe(II) quantum yield of Fe(Ox)$_2^-$ and Fe(Ox)$_3^{3-}$ is 1.17 and 0.91, respectively. The total Fe(II) quantum yield (Φ_{tot}) at 366 nm can be estimated by the following equation 8:

$$\Phi_{tot} = \sum_i \Phi_i \varepsilon_i f_i / \sum_i \varepsilon_i f_i \tag{8}$$

Where f_i, the molar fraction of a specific species i; ε_i, molar extinction coefficient of species i; Φ_i, individual quantum yield of species i for Fe(II) formation. $\Phi(Fe(Ox)^+)$ and $\varepsilon(Fe(Ox)^+)$ were estimated as 0 and 753 M^{-1} cm^{-1},[11,19] respectively. Other parameters were from refs. 19, 20.

Fig. S2 shows the estimated Φ_{tot} profile at different oxalate concentrations. At [Ox^{2-}]<50 μM (for 100 μM Fe(III)), [Ox^{2-}]<100 μM (for 200 μM Fe(III)) and [Ox^{2-}]<200 μM (for 400 μM Fe(III)), respectively, Φ_{tot} was extremely low and even lower than the control system (without oxalate ligand). A further increase in [Ox^{2-}], the corresponding Φ_{tot} gradually increased to the maximum value ($\approx$1.1). This result aligns well with the dependence of AO7 degradation rate on the total oxalate concentrations, as demonstrated in Fig.2. It implies that reactivity of PFS is strongly related to the Fe speciation and the photoreactivity of the prevalent Fe species. It also can be expected that photodegradation efficiency of PFS would greatly diminish as oxalate ligand is quickly depleted.
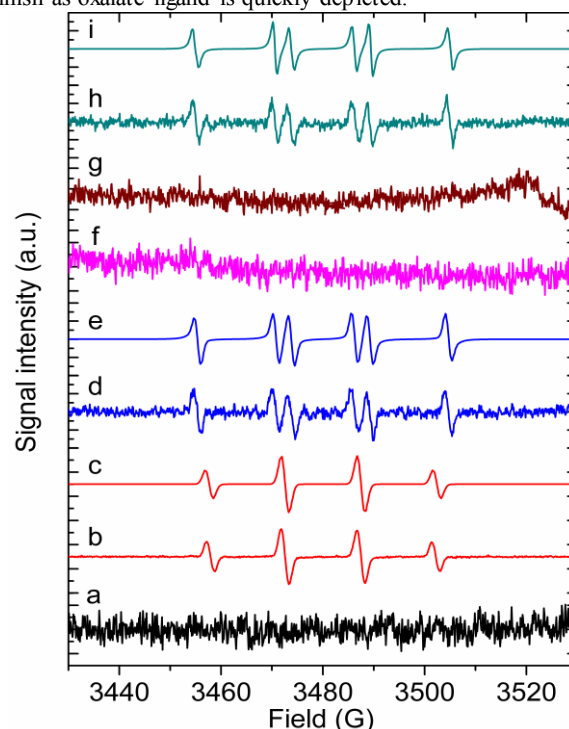
Fig. 4. ESR spectra of DMPO radical-adducts formed during the photolysis of Fe(III)/Ox solution under argon-purged conditions. DMPO, 0.04 M; pH, 3.0. (a) Ox only, 1000 μM. (b) Fe(III) only, 200 μM. (c) simulated data of b. (d) Fe(III), 200 μM; Ox, 100 μM. (e) simulated data of d. (f) Fe(III), 200 μM; Ox, 400 μM. (g) Fe(III), 200 μM; Ox, 1000 μM. (h) Fe(III), 100 μM; Ox, 1000 μM. (i) simulated data of h.

Free radicals involved

Photogeneration of Fe(II) may occur through two different ways: the primary photoreduction of Fe(III) complexes (Eqs. 1, 2) and the secondary reduction by the intermediate radical, such as CO$_2^{\cdot-}$ (Eq.3). Φ_{tot} for Fe(II) generation would be significantly affected by the competitive reaction of CO$_2^{\cdot-}$ with O$_2$. In contrast, excess Fe(III) (relative to O$_2$) would inhibit the formation of H$_2$O$_2$ by quenching

$CO_2^{\bullet-}$. Here ESR with DMPO as spin-trapping reagent was employed to determine reactive radicals involved in the reaction systems. To avoid the interference of dioxygen with carbon-centered radicals measurement, the ESR experiments were conducted under anaerobic conditions. As shown in Fig.4, two kinds of radicals were identified. The six-line ESR signal was assigned to DMPO-$CO_2^{\bullet-}$ adduct[22] (α_H=18.9 G, α_N=15.8 G) (Fig.4d, 4h), while the four-line one was known to be DMPO-$^{\bullet}OH$ (α_N=α_H=14.8 G)[23] (Fig. 4b). In the absence of oxalate, photolysis of hydroxylated Fe(III) complexes generates $^{\bullet}OH$ radicals (Fig. 4b). With addition of 100 μM oxalate, the signal of DMPO-$CO_2^{\bullet-}$ adduct appeared. According to Fig.3b, about 40% of Fe(III) was present as photo-inert Fe(Ox)$^+$, hydroxylated Fe(III) complexes being half of total Fe(III). Thus, $CO_2^{\bullet-}$ should not be originated from photolysis of Fe(Ox)$^+$, but from the attack of oxalate by photogenerated $^{\bullet}OH$ (Eq. 9).[24] Interestingly, a further increase of oxalate concentration (i.e. 400 μM and 1000 μM) led to disappearance of $CO_2^{\bullet-}$ signal (Fig. 4f, 4g). However, $CO_2^{\bullet-}$ was measurable in the presence of 100 μM Fe(III) and 1000 μM oxalate (Fig. 4h). This significant comparison indicates the yield of $CO_2^{\bullet-}$ was closely related to the abundance of Fe(III). DMPO might efficiently trap $CO_2^{\bullet-}$ at a lower Fe(III) content, but it is not the case at a higher level of Fe(III) where photoproduced $CO_2^{\bullet-}$ might be promptly captured by its adjacent Fe(III)-oxalato complexes.

$$C_2O_4^{2-} + {}^{\bullet}OH \longrightarrow CO_2^{\bullet-} + CO_2 + OH^- \qquad (9)$$
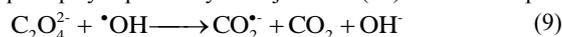
Conclusion

In this study, photochemistry of Fe(III)-oxalato complexes was investigated at varied levels of Fe(III) and oxalate. There was no measurable H_2O_2 accumulated at 200 μM Fe(III), partly due to the decrease of H_2O_2 formation resulted from $CO_2^{\bullet-}$ capture by excess Fe(III) and rapid consumption of H_2O_2 by photogenerated Fe(II). With the increase of oxalate concentration, photo-inert Fe(Ox)$^+$, most photoactive Fe(Ox)$_2^-$ and Fe(Ox)$_3^{3-}$ dominated the Fe(III) speciation and thus controlled the overall photochemical reactivity of Fe complexes. At Fe(III):oxalate<1:2, $^{\bullet}OH$ photoproduction efficiency, as probed by AO7 decoloration rate, was quite low compared with those with excess oxalate ligand. This result is very important for optimizing operation of photo/ferrioxalate system in its application of water treatment.

Acknowledgments

Notes and references

State Environmental Protection Engineering Center for Pollution Treatment and Control in Textile Industry, College of Environmental Science and Engineering, Donghua University, Shanghai, 201620, China

[*]*Corresponding author. fax +86-21-6779-2522. E-mail: zhaohuiwang@dhu.edu.cn (Z. Wang)*

Electronic Supplementary Information (ESI) available: [TOC result; Estimated quantum yield at 366 nm]. See DOI: 10.1039/c000000x/

1. M.E. Balmer and B. Sulzberger. *Environ. Sci. Technol.* 1992, **26**, 1014.

2. J. Jeong and J. Yoon. *Water Res.* 2005, **39**, 2893.

3. J. Jeong and J. Yoon. *Water Res.* 2004, **38**, 3531.

4. G. Liu, S. Zheng, X. Xing, Y. Li, D. Yin, Y. Ding and W. Pang. *Chemosphere* 2010, **78**, 402.

5. B. C. Faust and R. G. Zepp. *Environ. Sci. Technol.* 1993, **27**, 2517.

6. Y. Zuo and J. Hoigné. *Environ. Sci. Technol.* 1992, **26**, 1014.

7. J. Chen, H. Zhang, I. V. Tomov and P. M. Rentzepis. *Inorg. Chem.* 2008, **47**, 2024.

8. I. P. Pozdnyakov, O. V. Kel, V. F. Plyusnin, V. P. Grivin and N. M. Bazhin. *J. Phys. Chem. A* 2008, **112**, 8316.

9. Z. Wang, C. Chen, W. Ma and J. Zhao. *J. Phys. Chem. Lett.* 2012, **3**, 2044.

10. P. S. Surdhar, S. T. Mezyk and D. A. Armstrong. *J. Phys. Chem.* 1989, **93**, 3360.

11. L. Vincze and S. Papp. *J. Photochem.* 1987, **36**, 289.

12. Z. Wang, X. Chen, W. Ma, C. Chen and J. Zhao. *Environ. Sci. Technol.* 2010, **44**, 263.

13. H. Tamura, K. Goto, T. Yotsuyanagi and M. Nagayama. *Talanta* 1974, **21**, 314.

14. H. Bander, V. Sturzenegger and J. Hoigne. *Water Res.* 1988, 22, 1109.

15. Z. Wang, R. Yuan, Y. Guo, L. Xu and J. Liu. *J. Hazard. Mater.* 2011, **190**, 1083.

16. I. Puigdomenech. MEDUSA-Make Equilibrium Diagrams Using Sophisticated Algorithms. 2010. Available at: http://www.kemi.kth.se/medusa/.

17. D. L. Sedlak and J. Hoigné. *Atmos. Environ.* 1993, **27A**, 2173.

18. S. Hammami, N. Bellakhal, N. Oturan, M. A. Oturan and M. Dachraoui. Chemosphere 2008, **73**, 678.

19. C. Weller, S. Horn and H. Herrmann. *J. Photochem. Photobiol. A Chem.* 2013, **255**, 41.

20. B. C., Faust and J. Hoigné. *Atmos. Environ.* 1990, **24**, 79.

21. H-J. Benkelberg and P. Warneck. *J. Phys. Chem.* 1995, **99**, 5214.

22. F. A.Villamena, E.J. Locigno, A. Rockenbauer, C.M. Hadad and J.L. Zweier. *J. Phys. Chem. A.* 2006, **110**, 13253.

23. S. J. Klebanoff, A. M. Waltersdorph, B. R. Michel and H. Rose. *J. Biol. Chem.* 1989, **264**, 19765.

24. G. V. Buxton, C. L. Greenstock, W. P. Helman and A. B. Ross. *J. Phys. Chem. Ref. Data.* 1988, **17**, 513.

Table of Contents
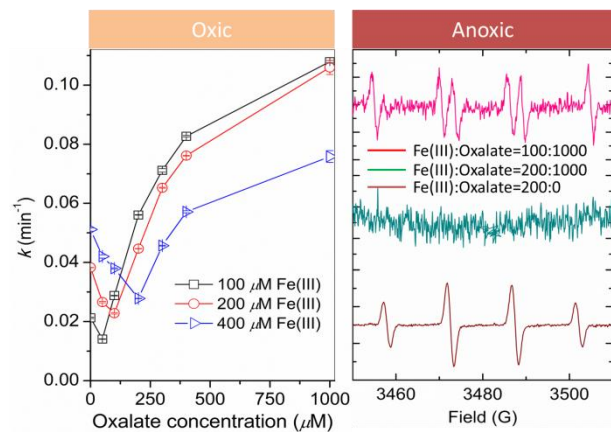
Text: Photoredox chemical behaviors of Fe(III)-oxalato complexes are strongly dependent on Fe(III) abundance and the nature of dominant Fe species.